

Response to Reviewer's Comments

The authors would like to thank the reviewer for the careful reading and constructive comments that have helped sharpen this manuscript. In this revision, all the comments of the reviewers have been carefully addressed. Specific responses to the review comments are listed below. The line numbers refer to those in the revised manuscript.

Anonymous Referee #1

1. Introduction: Pg 1_line 28 – Geological conditions here are referred to as an external factor influencing landslides. Geological conditions should be considered as an internal factor as is later suggested in the manuscript.

Response: Thank you for the careful reading. Indeed, geological conditions are considered as an internal factor in the manuscript. We have revised the manuscript accordingly. Please see **Introduction: Pg 1_lines 35-36** in this revision.

2. Introduction: Pg 1_line 31-35 – These final sentences of the first paragraph should really be the start of the introduction as this sets out the general motivation for the study before linking this to the site.

Response: Thank you for the careful reading and constructive comment. We agreed with the reviewer. We have revised the text accordingly. Please see **Introduction: Pg 1_lines 28-33** in this revision.

3. Introduction: Pg 2_lines 31-34 – I am not sure that this is needed I would suggest deleting this.

Response: Thank you for the comment. In this submission, we have revised the text accordingly. Please see **Introduction: Pg 2_lines 35-36** in this revision.

4. Methodology: Pg 2_lines 38-39 – I'm not sure I fully understand this point. Landslide displacement is caused by both internal and external factors but why does the lithology, geological structure and topography cause result in monotonic displacement through time? Also groundwater (pore water pressures) should be considered here. Most likely the ground water table remains high enough for ongoing movement to continue.

Response: Thank you for the careful reading and kind comment. To avoid the potential confusion, we have revised the text accordingly, with slight modification. Please see **2.1 Time series analysis of displacement: Pg 2_lines 41-46** in this revision.

The nonlinear evolution process of the cumulative displacement of landslides is controlled by primary factors such as geological conditions, and trigger factors such as rainfall and reservoir water level changes. The displacement of landslide sequence is an instability time series. Based on the time series analysis, total displacement of landslide can be broken down into different corresponding components according to the different influential factors. Total displacement of landslide can be divided into trend

component displacement, which is affected by the periodic dynamic functioning of inducing factors such as rainfall, reservoir water level, groundwater. Trend component displacement nearly increases under large time scales, and periodic component displacement fluctuated increases under small time scales. The trend component revealed the long-term trend of the sequence, which is determined by the potential energy and constraint condition of the slope.

Many landslides exhibit long-lasting, continuous movements under gravity loads that are affected by the creep property of slope materials (Desai et al. 1995). One of the important factors that influence the behavior of creeping slopes is appropriate characterization of the response of geologic materials and interfaces; in the case of creeping slopes, the latter can occur at the junction of the creeping mass and the essentially stationary (rock) mass below it. Landslide deformation is often characterized by creep, which generally need to undergo three stages, initial deformation, stable deformation and accelerated deformation stage. In the evolution scheme of three deformation phases of landslide, the landslide displacement generally increases monotonically with time.

Furthermore, we agreed with the reviewer that groundwater (pore water pressures) should be considered here. Groundwater, which is regarded as an active geologic agent, is one of the main factors that induces landslide instability. In the rising phase of reservoir water level, the groundwater level gradually increases, with a slight lag behind the increase in the reservoir water level. The groundwater remains high enough for ongoing movement to continue.

5. Methodology: Pg 5_lines 3-16 – This section This section introduces the GA computational model but largely explains this through its previous biological applications. It would be much easier for the reader to explain how this has been adapted for landslide studies.

Response: Thank you for the kind comment. We have revised the text accordingly.

We agreed with the reviewer that this section is not relevant to landslide, just introduces the GA model from the biological point of view. Thus, we deleted this section in the revision. About how this has been adapted for landslide studies, we had explained it in the introduction: Pg 2_lines 25-27.

6. Case Study: Pg 6_line 29 – Why is landslide monitoring considered a qualitative approach to analyse landslide development. This is quantitative data.

Response: Thank you for the careful reading and kind comment. We have revised the text accordingly. Indeed, landslide monitoring is considered a qualitative approach to analyse landslide development. We are very sorry for that our mistake in spelling words. Please see **Case Study: Pg 6_line 28** in this revision.

7. Case Study: Pg 8_lines 17-18 – This should be the other way around- the landslide stability decreased and the deformation increased.

Response: Thank you for the careful reading and kind comment. We have revised the text accordingly. Please see **Case Study: Pg 8_line 20-21** in this revision.

8. Case Study: Pg 9_line 24 – Statement ‘materials in the sliding mass are degraded by excess moisture and additional hydrodynamic pressure’ is not correct. The excess pore water pressure reduces the mean effective stress at the landslide shear surface making it more susceptible to movement.

Response: Thank you for the careful reading and constructive comments. We agreed with the reviewer about the explanation. We have revised the text accordingly. Please see **Case Study: Pg 12_line 23-24** in this revision.

9. Case Study: Pg 12_lines9-10 – How has the sliding force increased? Is it not the case that the confining pressure reduces with the lowering of the lake but the pore water pressure remains high so this change in stress state makes the slope more unstable?

Response: Thank you for the constructive comments. We have revised the text accordingly. Please see **Case Study: Pg 12_line 5-13** in this revision for details.

Although the variation in reservoir water level was small before April 2007, the periodic displacement still exhibited small fluctuations due to the effects of rainfall and groundwater. This behavior could be explained in terms of stress changes within the landslide in that the rainfall events cause increased pore water pressures in the landslide shear zone which reduced the effective stress and increased instability. After April 2007, several distinct peaks can be observed in the periodic displacement-time curves during periods of decreasing reservoir water level. For example, the periodic displacement increased from May to July 2009 and from May to September 2012. However, when the reservoir water level increased from 145 m to 175 m, the periodic displacement gradually decreased. The main reason for the above conditions was that the rise of the reservoir water level increased the confining stress on the surface of the landslide and the hydrodynamic pressure, the direction of which was toward the interior of sliding body. Similarly, the lowering of the reservoir water level reduced the confining stress whilst pore water pressures were still high which would promote accelerated movement.

10. Case Study: Pg 12_line 12 – Is this an actual piezometer or standpipe installation or is this water observed within the inclinometer tube itself? If the latter is there any certainty as to where this has come from? If not an installed piezometer it could have come from the top cap of the installation and therefore may not be a reliable groundwater measurement.

Response: Thank you for the careful reading and constructive comments. We have revised the text accordingly. Please see **Case Study: Pg 12_line 15-16** in this revision for details.

The water gauge used in this landslide was 730 type water level sensor, with the characteristics of measuring range as deep as 210 meters, high measuring accuracy and stable performance. The data acquisition and memory used NetL G-301 data storage device. At the head scarp of the landslide at an elevation of 181m, groundwater depth was measured by water gauge within inclinometer monitoring hole QZK3.

11. Figures Fig 4. The key is not explained. A clear key showing instrument type and borehole

locations is needed Fig 5. As with figure 4 the key is not clear. Also the borehole and inclinometers should be drawn on to show their depth. Fig 8. Diagrams are hard to read. It would be better to display these as conventional inclinometer plots with depth on the y axis and displacement on the x axis.

Response: Thank you for the careful reading and constructive comments. We have revised the text accordingly.

About Fig. 4 and Fig.5, we have added the key for legend information accordingly. Please see **Fig.4** and **Fig.5** in this revision for details.

Furthermore, Fig 8. Diagrams is displayed as conventional inclinometer plots with depth on the y axis and displacement on the x axis. Please see **Fig 8** in this revision.

References

Furuya, G., Sassa, K., Hiura, H., Fukuoka, H.: Mechanism of creep movement caused by landslide activity and underground erosion in crystalline schist, Shikoku Island, southwestern Japan, Eng Geol, 53, 311-325, 10.1016/S0013-7952(98)00084-2, 1999.

Desai, C. S., Samtani, N. C., Vulliet, L.: Constitutive modeling and analysis of creeping slopes, J Geotech Eng Trans ASCE, 121,43-56, 10.1061/(ASCE)0733-9410(1995)121:1(43), 1995.

Sun, M., Tang, H., Wang, M., Shan, Z., Hu X.: Creep behavior of slip zone soil of the Majiagou landslide in the Three Gorges area, Environ Earth Sci, 16, 1-12, 10.1007/s12665-016-6002-x, 2016.

Haq, A. N., Marimuthu, P., Jeyapaul, R.: Multi response optimization of machining parameters of drilling Al/SiC metal matrix composite using grey relational analysis in the Taguchi method, The Int J Adv Manuf Technol, 37, 250-255, 10.1007/s00170-007-0981-4, 2008.

1 **Landslide displacement prediction using the GA-LSSVM model and time series analysis: a case study**
2 **of Three Gorges Reservoir, China**

3 Tao Wen¹, Huiming Tang^{1,2*}, Yankun Wang², Chengyuan Lin¹, Chengren Xiong²

4 1 Faculty of Engineering, China University of Geosciences, Wuhan 430074, Hubei, People's Republic of China; 2 Three Gorges
5 Research Center for Geo-hazards of Ministry of Education, China University of Geosciences, Wuhan, Hubei 430074, People's
6 Republic of China

7 *Corresponding author: tanghm@cug.edu.cn

8
9 **Abstract** Predicting landslide displacement is challenging, but accurate predictions can prevent casualties and economic losses.
10 Many factors can affect the deformation of a landslide, including the geological conditions, rainfall, and reservoir water level.
11 Time series analysis was used to decompose the cumulative displacement of landslide into a trend component and a periodic
12 component. Then the least squares support vector machine (LSSVM) model and genetic algorithm (GA) were used to predict
13 landslide displacement, and we selected a representative landslide with **episodic movement** deformation as a case study. The trend
14 component displacement, which is associated with the geological conditions, was predicted using a polynomial function, and the
15 periodic component displacement which is associated with external environmental factors, was predicted using the GA-LSSVM
16 model. Furthermore, based on a comparison of the results of the GA-LSSVM model and those of other models, the GA-LSSVM
17 model was superior to other models in predicting landslide displacement, with the smallest root mean square error (*RMSE*) of
18 62.4146 mm, mean absolute error (*MAE*) of 53.0048 mm, and mean absolute percentage error (*MAPE*) of 1.492% at monitoring
19 station ZG85, while these three values are 87.7215 mm, 74.0601 mm and 21.1.703% at ZG86 and 49.0485 mm, 48.5392 mm and
20 3.131% at ZG87. The results of the case study suggest that the model can provide good consistency between measured
21 displacement and predicted displacement, and periodic displacement exhibited good agreement with trends in the major
22 influencing factors.

23 **Keywords** landslide; displacement prediction; least squares support vector machine; genetic algorithm; reservoir water level;
24 rainfall

25 **1 Introduction**

26 In the Three Gorges Reservoir region, landslides are the main type of geo-hazard, and they cause critical harm to individuals
27 and property each year (Du et al. 2013; Yao et al. 2013; Lian et al. 2014; Cao et al. 2016). The **displacement prediction of**
28 **landslides** is a major focus in the field of **landslide research** (Sassa et al. 2009; Du et al. 2013). Comprehensive analyses of
29 **landslide response** and **displacement predictions of landslide** based on external factors are effective methods that rely on **landslide**
30 **deformation data**. The **evolution process of landslide** is a complex non-linear process caused by the **complex interaction of**
31 **different factors**. The **accurate prediction of reservoir landslide processes** is an important basis for early prevention, and it can
32 **reduce the loss of property and lives** (Corominas et al. 2005). Therefore, geological surveying, monitoring, landslide prevention
33 and landslide prediction must be improved to **minimise** the losses caused by landslides (Kirschbaum et al. 2010; Miyagi et al. 2011;
34 Ahmed 2013). A landslide can be regarded as a nonlinear and dynamic system that is affected by **external factors, such as rainfall,**
35 **reservoir water levels, groundwater, etc.** (Guzzetti et al. 2005; Kawabata and Bandibas 2009). Due to the influences of external
36 factors, deformation displacement of landslide generally exhibits the same tendencies as the variations in external factors, which
37 can result in misleading landslide prediction. **Displacement time series is usually considered as a direct representation of complex**
38 **nonlinear dynamical behavior of landslide.**

39 In recently years, grey system models, time series models, neural network models, extreme learning machines, support
40 vector machines (SVM), etc. have been widely used for **landslide displacement prediction** (Wang 2003; Pradhan et al. 2014;
41 Gelisli et al. 2015; Goetz et al. 2015; Kavzoglu et al. 2015). Previously, landslide susceptibility maps were assessed using a back
42 propagation artificial neural network and logistic regression analysis (Nefeslioglu et al. 2008). Additionally, dynamic time series
43 predictors were proposed based on echo state networks (Yao et al. 2013). Lian et al. (2013) used an extreme learning machine and
44 ensemble empirical mode decomposition to predict landslide displacement. Although these models were constructed based on
45 ensemble empirical mode decomposition to predict landslide displacement. Although these models were constructed based on

1 different algorithms, each has strengths and weaknesses. Grey system models are widely used in analyses of exponential time
2 series. However, for complex nonlinear slope displacement series, prediction results can yield considerable error (Yin and Yu 2007;
3 Sun et al. 2008). Additionally, autocorrelation coefficients, partial correlation coefficients and pattern recognition features are
4 difficult to determine via time series analysis (Brockwell and Davis 2013; Turner et al. 2015). The neural network method is a
5 powerful tool in landslide prediction (Liu et al. 2014; Lian et al. 2015). However, the conventional neural network has many
6 limitations, including overfitting and a shortage of theoretical guidance in the selection of the number of network nodes in the
7 hidden layer, which diminishes its prediction ability (Hwang et al. 2014). In addition, the neural network neglects practical issues
8 by using a pre-defined activation function. Compared with traditional learning algorithms, although extreme learning machines are
9 characterized by high generalization, good performance and fast computing speed, their output is different at different times due to
10 the use of randomly selected input (Lian et al. 2014). Thus, it is difficult to reflect large quantities of information completely and
11 predict landslide displacement accurately using these models because landslide displacement is actually a finite time series.

12 The SVM model can effectively overcome the limitations of other methods, including small sample sizes, high
13 dimensionality and nonlinearity. Many studies have illustrated the ability of SVM models to recognize learning patterns, such as
14 nonlinear regression, and obtain the global optimum solutions to these problems (Feng et al. 2004; Marjanović et al. 2011;
15 Micheletti et al. 2011; Hong et al. 2016). Although these problems can be transformed into quadratic convex programming
16 problems, the computation speed of the SVM model is slow when the training data set is large or the dimensionality is high (Zhang
17 et al. 2009). To overcome these inadequacies, we use the least squares support vector machine (LSSVM) proposed by Suykens and
18 Vandewalle (1999), which is a supervised learning model that has been widely applied in other machine learning problems, such as
19 function fitting. The LSSVM model uses the square sum of the least square linear system error as the loss function and solves the
20 problem by transforming it into a set of equations, which increases the solution speed and reduces the required calculation
21 resources (Suykens et al. 2002; Lv et al. 2013; Xu and Chen 2013; Zhang et al. 2013). Additionally, this method yields good
22 performance in pattern recognition and nonlinear function fitting. However, the selection of parameters is crucial to developing an
23 efficient LSSVM model due to its sensitivity to small variations in the parameters.

24 The genetic algorithm (GA) is a global optimization algorithm that uses highly parallel, random and adaptive searching
25 based on biological natural selection and optimization. Thus, the method is particularly suitable for solving complex and nonlinear
26 problems (Li et al. 2010; Ali et al. 2013). In this paper, the GA is selected as the method of parameter optimization in the LSSVM
27 due to its advantages in determining the unknown parameters that are consistent between the predicted data and the measured data.
28 By introducing the GA, some key parameters of the LSSVM model can be derived automatically. Therefore, we select the
29 combination of the LSSVM model and the GA to predict landslide displacement.

30 Due to the influences of rainfall, reservoir water level and human activities on the monitoring data of landslide displacement,
31 most monitoring data series are incomplete or highly variable. These issues introduce uncertainty into the mathematical model and
32 increase the difficulty of prediction. To overcome this and obtain the main error sources, a time series analysis of displacement is
33 conducted by decomposing the monitoring data series into several components (Du et al. 2013). Then, the monitoring data series
34 are simulated using the moving average method. **Shuping landslide, a typical landslide with episodic movement deformation, was**
35 **taken as an example to validate and the GA-LSSVM model with time series analysis.**

36 **2 Methodology**

37 **2.1 Time series analysis of displacement**

38 Cumulative displacement of landslides is caused by the combined effects of internal geological conditions (lithology,
39 geological structure, topography, etc.) and external environmental factors (rainfall, reservoir water level, groundwater, etc.). The
40 displacement of landslide sequence is an instability time series. The landslide displacement caused by the former increases
41 generally with time, which reflects the trend in cumulative displacement. Landslide deformation exhibit long-lasting and
42 continuous movements under gravity loads that is affected by the creep characteristic (Desai et al. 1995). One of the important
43 reasons that influence the creep behavior is the expression of the response of geological materials and interfaces. Landslide
44 deformation is often characterized by creep, which generally need to undergo three stages, initial deformation, stable deformation
45 and accelerated deformation stage. However, the landslide displacement induced by the latter is approximately periodic. Therefore,
46 a landslide displacement sequence is an instability time series with a periodic episodic movement characteristic. According to time

1 series analysis, cumulative displacement can be decomposed into three portions as follows:

2

$$y_t = p_t + q_t + \varepsilon_t \quad (1)$$

3 where y_t is the cumulative displacement, p_t is the trend component displacement, q_t is the periodic component displacement,
4 and ε_t is the random component displacement.

5 However, it is difficult to obtain relevant data regarding the random component (wind loads, car loads, etc.) due to the lack
6 of advanced monitoring methods. In this paper, the random component displacement is not considered. Therefore, we can simplify
7 the time series model as follows.

8

$$y_t = p_t + q_t \quad (2)$$

9 The trend component can be extracted using the moving average method as follows:

10

$$A_i = \{a_1, a_2, \dots, a_j, \dots, a_n\} \quad (3)$$

11

$$\overline{p}_t = \frac{a_t + a_{t-1} + \dots + a_{t-k-1}}{k} (t = k, k+1, \dots, n) \quad (4)$$

12 where A_i is the time series of cumulative displacement of the i th monitoring system ($i=1, 2, \dots, m$), a_j is the cumulative
13 displacement of the i th monitoring system at time j ($j=1, 2, \dots, n$), \overline{p}_t is the extracted value of the trend component, and k is the
14 moving average period.

15 The periodic component displacement can be acquired by subtracting the trend component displacement from the
16 cumulative displacement. Therefore, the time series model not only reflects the relationship between each component of
17 cumulative displacement but also provides mathematical and physical meaning for landslide displacement prediction.

18 2.2 LSSVM

19 The LSSVM model is a regression prediction method with nonlinear characteristics based on a statistical learning theory,
20 and it is regarded as an improved form of the SVM (Vapnik 1995; Abdi and Giveki 2013). First, after dividing the sample data
21 into training samples and testing samples, the training samples are plotted in a high-dimension feature space via nonlinear mapping.
22 Then, the optimal decision function model is obtained for the best-fitted results by training the sample data $\{x_j, y_j\}$, where $j=1, 2,$
23 $3, \dots, n$. The regression function of the LSSVM can be expressed as follows:

24

$$f(x) = W^T \varphi(x) + b \quad (5)$$

25 where W^T is the weight vector, $\varphi(x)$ is a nonlinear mapping function that maps the sample data into the feature space, x is the
26 input, y is the output, and b is the offset.

27 By searching or a function $f(x)$ that adjusts the dispersion degree of the training samples, we can obtain a risk-minimized
28 solution. This solution can be written using the structural risk minimization principle:

29

$$\text{Minimize: } \frac{1}{2} W^T W + \frac{C}{2} \sum_{j=1}^n \xi_j^2 \quad (6)$$

30

$$\text{Subject to: } y_j = W^T \varphi(x_j) + b + \xi_j \quad (j=1, 2, \dots, n) \quad (7)$$

31 where C is a penalty factor representing the penalty degree of the training samples, b is the offset, and ξ_j is the relaxation factor.

1 Based on the Lagrange equation and duality theory, the optimization problem can be converted into a dual problem:

2

$$L(W, b, \xi, \alpha) = \frac{1}{2} W^T W + \frac{C}{2} \sum_{j=1}^n \xi_j^2 - \sum_{j=1}^n \alpha_j (W^T \varphi(x_j) + b + \xi_j - y_j) \quad (8)$$

3 where α_j is the Lagrange multiplier.

4 The solution of the optimization equation is obtained by solving the partial differential form of the Lagrange equation with
5 respect to W , b , ξ_j , α_j . The optimization equations are expressed as follows.

6

$$\begin{cases} \frac{\partial L}{\partial W} = 0 \Rightarrow W = \sum_{j=1}^n \alpha_j y_j \varphi(x_j) \\ \frac{\partial L}{\partial b} = 0 \Rightarrow \sum_{j=1}^n \alpha_j y_j = 0 \\ \frac{\partial L}{\partial \xi_j} = 0 \Rightarrow \alpha_j = C \xi_j \\ \frac{\partial L}{\partial \alpha_j} = 0 \Rightarrow y_j [W^T \varphi(x_j) + b] - 1 + \xi_j \end{cases} \quad (9)$$

7 The linear equations can be obtained by solving Eq. (9) with the elimination of W and ξ :

8

$$\begin{bmatrix} 0 & I^T \\ I & ZZ^T + C^{-1}E \end{bmatrix} \begin{bmatrix} b \\ \alpha \end{bmatrix} = \begin{bmatrix} 0 \\ y \end{bmatrix} \quad (10)$$

9 where $y = [y_1, y_2, \dots, y_l]^T$, $I = [1, \dots, 1]^T$, $\alpha = [\alpha_1, \alpha_2, \dots, \alpha_l]^T$, $Z = [\varphi(x_1), \varphi(x_2), \dots, \varphi(x_l)]^T$ and E is the unit
10 matrix with l dimensions.

11 Then, the regression prediction model of the LSSVM can be rewritten based on the above optimization problem:

12

$$f(x) = \sum_{j=1}^n \alpha_j K(x, x_j) + b \quad (11)$$

13 where $K(x_j, x)$ is a kernel function.

14 In the paper, we select the radial basis kernel function as the kernel function in the LSSVM model to obtain the optimal
15 solutions due to its strong nonlinear mapping ability and wide convergence domain (Min and Lee 2005; Altinel et al. 2015; Elbisy
16 2015; Farzan et al. 2015):

17

$$K(x_j, x) = \exp(-(x - x_j)^2 / (2\sigma^2)) \quad (12)$$

18 where σ is a parameter of the kernel function.

19 The parameter of the model C and the parameter of the kernel function σ significantly influence the prediction
20 performance. The parameter C represents the error tolerance. The more accurate the parameter is, the higher the prediction
21 performance is, but this can lead to overtraining. The parameter σ implicitly determines the spatial distribution of data mapping
22 in the new feature space. Therefore, some measures should be taken to optimize the LSSVM parameters.

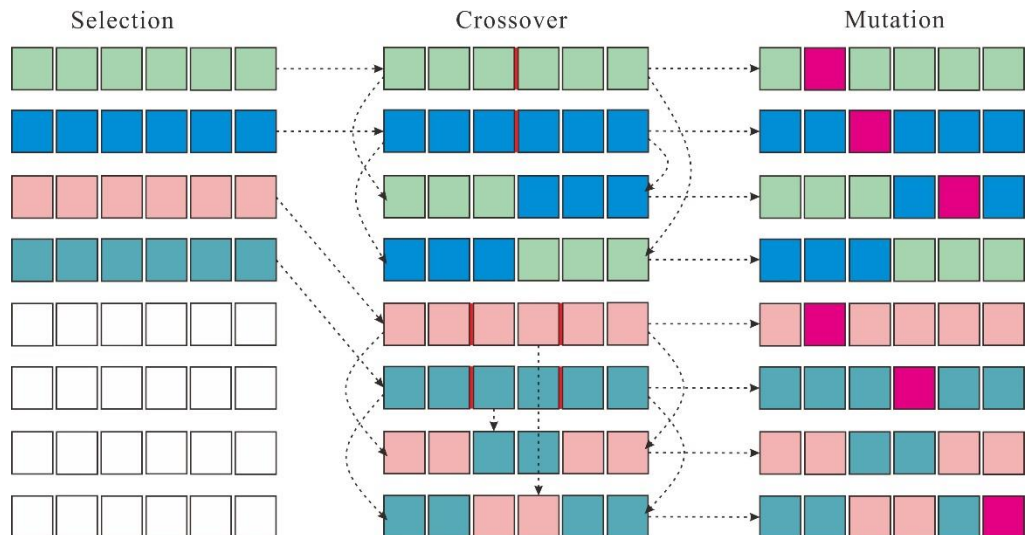
23 **2.3 GA**

24 Currently, several intelligent algorithms are used to solve optimization problem, such as the GA (Li et al. 2010; Ali et al.
25 2013), grid algorithm (Lin 2001), particle swarm optimization (Vandenberghe and Engelbergh 2006) and genetic programming
26 (Garg and Tai 2011; Shen et al. 2012). However, compared with the GA, the grid algorithm is tedious and cannot yield satisfactory

1 results (Gu et al. 2011). For discrete optimization problems, particle swarm optimization performs poorly and often yields local
 2 optima (Fei et al. 2009). In addition, genetic programming, which was developed by Koza (1992), provides solutions to complex
 3 problems using evolutionary algorithms, and the method is typically expressed as a tree structure that consists of terminals and
 4 functions; however, it is difficult to generate new individuals, which seriously affects the convergence rate (Garg et al. 2014). In
 5 this paper, we select the GA to determine the best parameters (C and σ) of the LSSVM for predicting landslide displacement.

6 The GA is a computational model **commonly used to simulate** natural selection and the biological evolution processes of
 7 genetic mechanisms. The GA provides solutions for complicated problems using evolutionary algorithms (Levasseur et al. 2008;
 8 Hejazi et al. 2013). The typical genetic operations include selection, crossover and mutation.

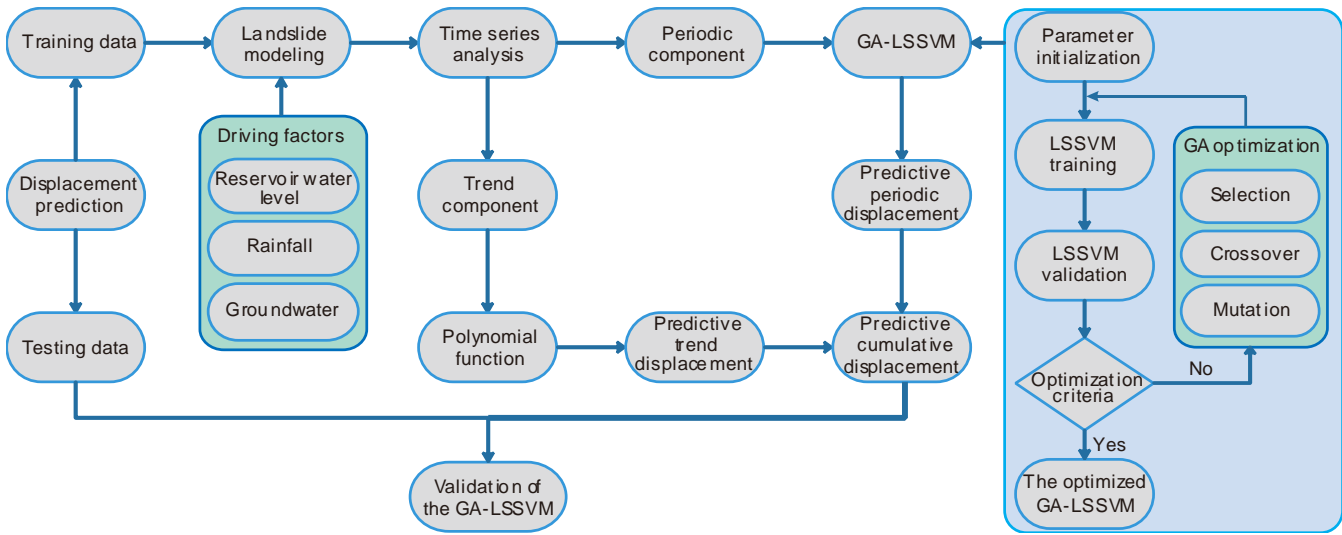
9 Based on certain methods and theories, selection operations, such as the fitness-ratio selection algorithm, ranking algorithm,
 10 Monte Carlo selection and tournament selection, are commonly used to choose a parental generation from a population based on
 11 an individual's fitness value. Crossover operation can generate two new offspring by selecting random codes from two parents and
 12 then exchanging their respective branches. Point mutation is commonly used as the mutation operator. By selecting a random node
 13 from a parent, a new individual is generated by substituting the selected random node into another parent branch. A typical genetic
 14 algorithm is shown in Fig. 1. Selection operations, crossover operations and mutation operations are probabilistic, and with a
 15 probability of over 90%, crossover operations are the most widely used.



16
 17 Fig. 1 Diagram of genetic operations

18 **2.4 GA-LSSVM model**

19 To obtain the best model, the parameters of the model must be carefully selected in advance (Duan et al. 2003). According
 20 to some research results (Lessmann et al. 2005; Pourbasheer et al. 2009), the GA has the advantages of reducing the blindness of
 21 artificial selection and enhancing the discrimination ability of the LSSVM model. Modeling with this method can achieve high
 22 precision if the training samples are reliable. The sampling data used for landslide displacement prediction are continuous and
 23 mutually dependent landslide data applicable for a specific method; thus, the data are essentially independent sampling data.
 24 In this paper, the periodic component displacement is predicted by the GA-LSSVM model, which has higher accuracy than other
 25 models due to the consideration of the trigger factors. MATLAB software is used to execute the model. The flowchart of the
 26 GA-LSSVM model is presented in Fig. 2.



1
2 Fig. 2 The basic flowchart of the GA-LSSVM model, including the establishment of the GA-LSSVM model and the validation of
3 the model

4 3 Case study: Shuping landslide

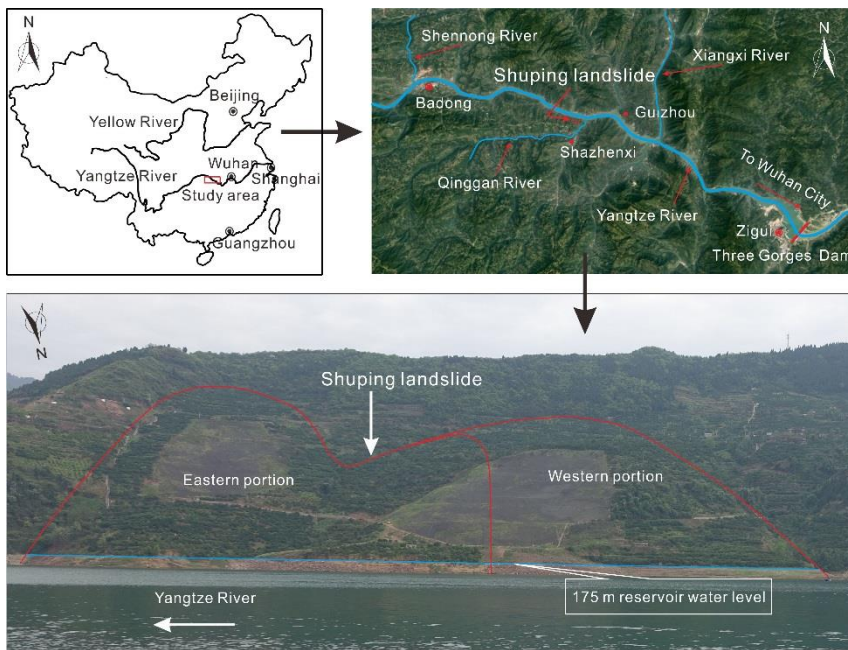
5 3.1 Geological conditions

6 The Shuping landslide is located in Shazhenxi town, Zigui country, Hubei province, China, near the Yangtze River and
7 approximately 47 km into the upper reach of Three Gorges Dam (Fig. 3). The sliding direction of Shuping landslide is N11°E, and
8 the landslide presents a sector in a topographic map (Fig. 3). The reservoir water level in Fig. 3 is 166 m. The topography is
9 relatively flat, with a mean slope angle of 22°. The highest elevation of the landslide is 400 m above sea level. The head scarp of
10 the landslide reaches to the riverbed of the Yangtze River at 60 m in elevation. The landslide covers an area of approximately
11 $54 \times 10^4 \text{ m}^2$, with an average length of 800 m in the longitudinal direction and an average length of 670 m in the transverse direction.
12 The landslide volume is $2070 \times 10^4 \text{ m}^3$, with an average sliding surface depth of 40 m (Fig. 4). Fig. 4 shows the eight GPS
13 monitoring stations installed on the ground surface of the landslide, as well as four inclinometers monitoring holes. The bedrock is
14 mainly sandy mudstone. The strata comprise the Triassic Badong formation. The dip direction of the bedrock is between 120° and
15 165°, and the dip angle is between 10° and 35°. The landslide is divided into an eastern portion and a western portion, and the
16 materials of the landslide mainly include Quaternary deposits and soils containing silty clay and rock fragments with a loose and
17 disorderly structure (Fig. 5). Fig. 5 shows a longitudinal section of the eastern portion. The sliding surface is steep in the upper
18 area, which is located between the deposits and the bedrock.

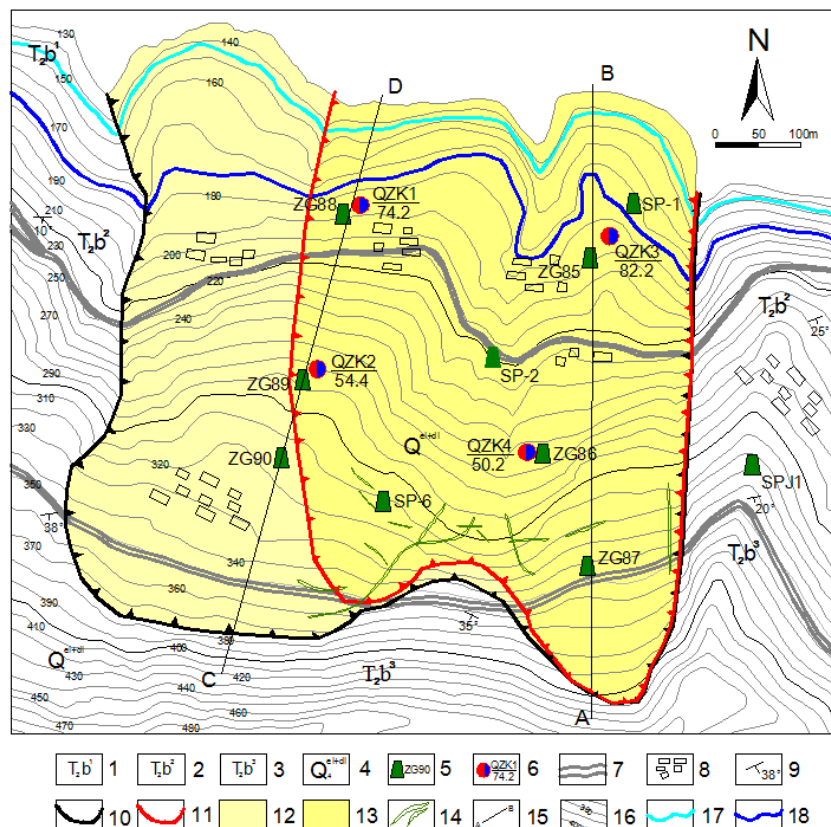
19 Underground moisture beneath the landslide is primarily **ground** water flowing through a loose medium that consists of
20 colluviums, deposits, etc. After the water storage began in Three Gorges Reservoir in June 2003, the landslide deformation became
21 more active. Various external factors affect the landslide displacement, including rainfall, the reservoir water level, surface water
22 infiltration, groundwater, etc.

23 3.2 Monitoring data and deformation characteristics of the landslide

24 Field investigations revealed that there was no obvious deformation of this landslide before the first impoundment of the
25 reservoir on June 15, 2003. However, **cracking** occurred through roads and houses, after the first impoundment. To measure the
26 deformation characteristics and stability of the landslide, monitoring stations were **installed** to observe the interactions between
27 different portions of the landslide. The monitoring methods include geodetic surveys, drilling, meteorological observations and
28 geological investigations. Thus, the development processes and evolution of the landslide can be analyzed **quantitatively** using
29 monitoring data from eight monitoring stations and four inclinometer monitoring holes located along the longitudinal direction of
30 the landslide (ZG85 to ZG90, SP-2 and SP-6, QZK1 to QZK4 in Fig. 4).



1
2 Fig. 3 Location of the study area and panorama of the Shuping landslide and landslide subzones



3
4 Fig. 4 Geology and deformation monitoring map of Shuping landslide. 1 Middle Triassic Badong Formation Section 1, 2 Middle
5 Triassic Badong Formation Section 2, 3 Middle Triassic Badong Formation Section 3, 4 Quaternary colluviums, 5 GPS
6 monitoring stations and number, 6 inclinometer monitoring hole and its depth (the unit of depth is the meter), 7 roads, 8 houses, 9
7 lithology orientation, 10 landslide boundary, 11 main sliding boundary, 12 western portion zone, 13 eastern portion zone, 14
8 cracks, 15 longitudinal section, 16 counter line, 17 reservoir water level (145 m), and 18 reservoir water level (175 m)

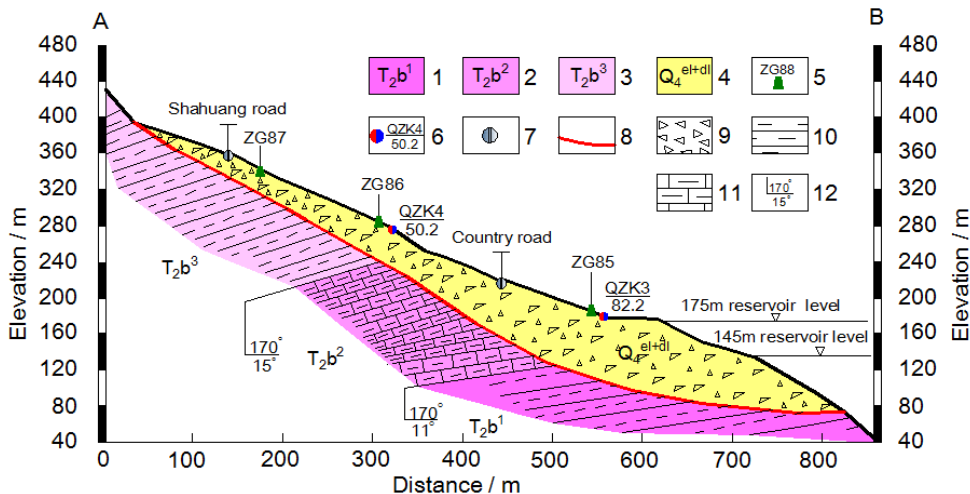
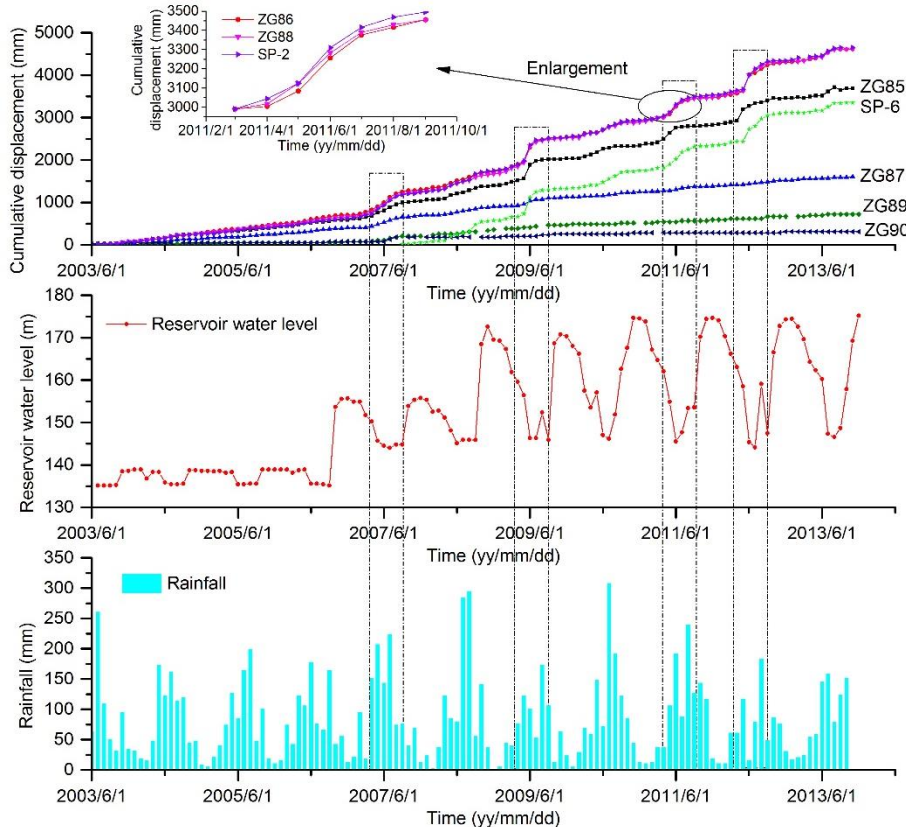


Fig. 5 Geological longitudinal section (line A-B in Fig. 4) of Shuping landslide. 1 Middle Triassic Badong Formation Section 1, 2 Middle Triassic Badong Formation Section 2, 3 Middle Triassic Badong Formation Section 3, 4 Quaternary colluviums, 5 GPS monitoring stations and number, 6 inclinometer monitoring hole and its depth (the unit of depth is the meter), 7 roads, 8 sliding zone, 9 colluvial gravel soil, 10 silty mudstone, 11 argillaceous limestone, and 12 lithology orientation

Fig. 6 shows the monitoring results between July 2003 and October 2013, including rainfall and reservoir water level, which exhibit near **episodic movement** characteristics after the first impoundment. The displacements in the middle (ZG86) and head scarp (ZG85) areas were greater than that in the back scarp (ZG87) area of longitudinal section A-B, and the displacements in the head scarp (ZG88) and middle (ZG89) areas were greater than that in the back scarp (ZG90) area in the western zone. These observations suggest that **landslide displacements** increased steadily, and Shuping landslide displayed retrograde style deformation from the lower part to the upper part. The cumulative displacements at the monitoring stations located in the frontal areas were relatively low, with an average value of 880 mm, and the cumulative displacements at the monitoring stations located in the middle-rear areas were very high, with an average value of 3890 mm. Overall, landslide deformation in the eastern zone was greater than that in the western zone. Based on the reservoir water level data and the displacements measured at eight monitoring stations, the cumulative displacement rate increased after the initial impoundment. Due to the increased rainfall and decreased reservoir water level between April and August each year, the cumulative displacement rises rapidly. Notable **landslide accelerations** can be observed in 2007, 2009, 2011 and 2012. The variations in reservoir water level and heavy rainfall **increase pore water pressure and reduce the effective stress in the slope**. In addition, the uplift pressure, hydrostatic pressure and hydrodynamic pressure acting on the landslide changed periodically. As a result, **the landslide stability decreased and the deformation increased**.



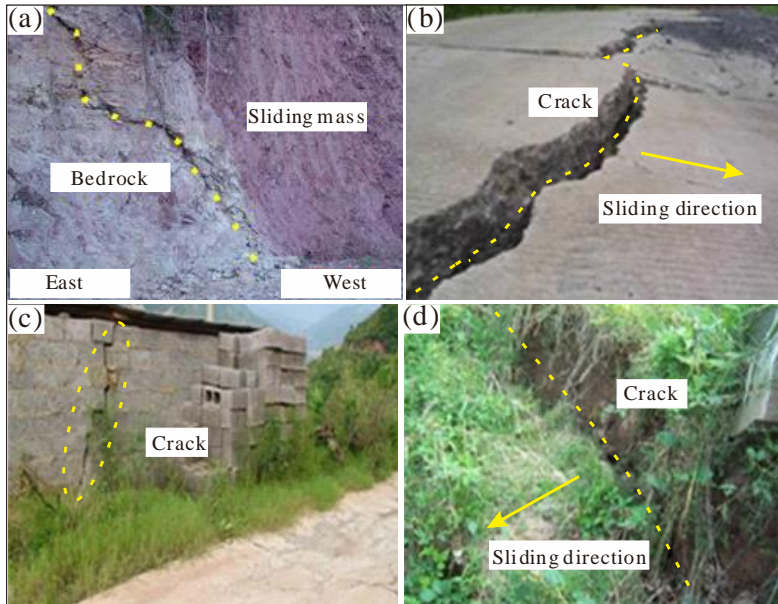
1
2 Fig. 6 The relationships between rainfall, reservoir water level and displacement

3 Many deformation or failure phenomena were observed in the Shuping landslide. In June 2003, a crack was generated in the
4 middle part of the landslide on the outside of a local road, as shown in Fig. 7(a). In 2006, the reservoir water level increased to 156
5 m for the first time. Fig. 7(b) illustrates that the crack gradually extended to a width of 10 cm within 3 months of completing
6 the road in April 2007. In August 2008, after a heavy storm occurred, deformation and tension cracks developed in the eastern portion
7 of the landslide and impacted houses, as shown in Fig. 7(c). Since 2008, the reservoir water level has increased gradually to 172 m
8 in October. In June 2009, the western portion of the landslide started cracking, with a maximum crack width of 20 cm and depth of
9 20-50 cm. In addition, several tension cracks formed at the eastern landslide boundary. The tension cracks in the eastern portion
10 are shown in Fig. 7(d). In recent years, the cumulative deformation rate has remained low due to the relatively stable reservoir
11 water level, which has fluctuated between 145 m and 175 m.

12 Therefore, the landslide deformation characteristics suggest that deformation in the western portion of the landslide is
13 smaller than that in the eastern portion, and the Shuping landslide is affected by reservoir water level fluctuations and rainfall.
14 When rainfall increases abruptly and the reservoir water level drops between April and August annually, the landslide becomes
15 active, which increases landslide deformation. In other conditions, the landslide undergoes slow deformation at a constant speed.

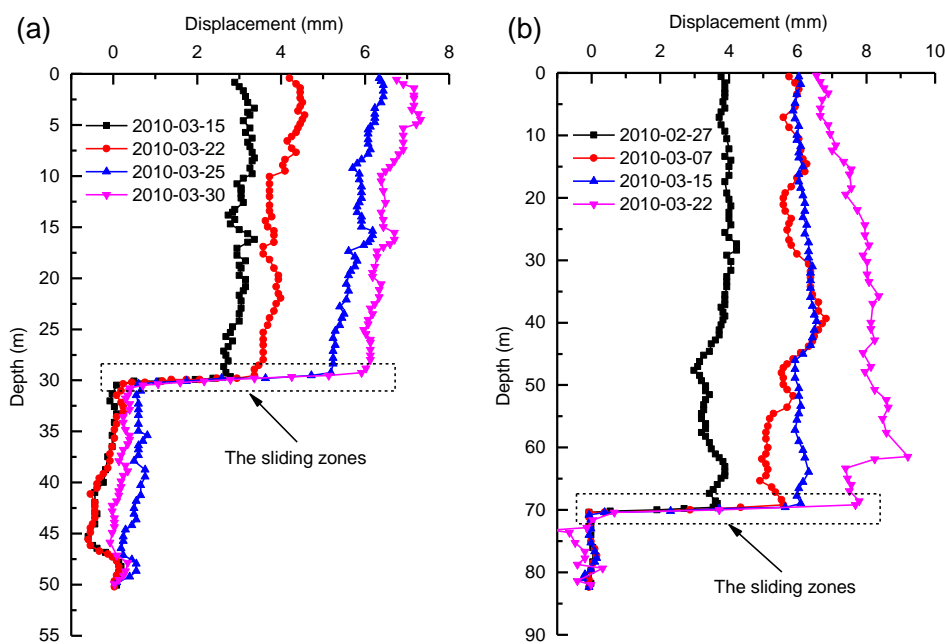
16 In addition, groundwater, which is regarded as an active geologic agent, is one of the main factors that induces landslide
17 instability. In the rising phase of reservoir water level, the groundwater level gradually increases, with a slight lag behind the
18 increase in the reservoir water level. The groundwater remains high enough for ongoing movement to continue. Conversely, the
19 groundwater level decreases in the declining phase of the reservoir water level. Moreover, the uplift pressure and seepage force of
20 groundwater are dynamic processes that affect landslide stability. Therefore, groundwater influences displacement.

21 Overall, the reservoir water level, rainfall and groundwater are the major factors that influence the displacement of the
22 Shuping landslide. The landslide displacement obviously increases when the reservoir water level decreases or when rainfall is
23 heavy and continuous because the excess pore water pressure reduces the mean effective stress at the landslide shear surface
24 making it more susceptible to movement.



1
2 Fig. 7 Photographs of the ground cracks in the landslide (Ren et al., 2015): (a) crack in the middle of the landslide on the outside
3 of the local road, (b) failure state of the local road, (c) wall cracking and subsidence in the eastern portion, and (d) the tension
4 cracks in the eastern portion

5
6 During the period between June 2003 to June 2009, monitoring data show that the landslide deformation differences are
7 manifested in the ground surface, and they display vertically distributed characteristics with elevation. In conclusion, the surface
8 displacements below 200 m in elevation are larger than those above 200 m, and deformation is largest close to 175 m, which is the
9 upper limit of the reservoir water level. This observation is due to the considerable influence of fluctuations in the reservoir water
10 level on the landslide area below 200 m. The deep deformation of the landslide exhibited distinct differences at different depths, as
11 shown in Fig. 8. Inclinometer monitoring holes QZK3 and QZK4, QZK1 and QZK2, which are located in the western portion of
12 the landslide, exhibited small deformation and similar deformation trends. Thus, their lateral displacement curves are not presented,
13 and only the curves of QZK3 and QZK4 are illustrated in this paper. The figures show that the sliding zones of QZK3 and QZK4
14 are located at elevations of 70 m and 30 m, respectively. Furthermore, the displacement change in the shallow sliding zones of
15 both QZK3 and QZK4 is larger than that in the deep sliding zone.



16
17 Fig. 8 Lateral displacements of Shuping landslide: (a) inclinometer monitoring hole QZK3 and (b) inclinometer monitoring hole

1 QZK4

2 **4 Landslide displacement prediction**

3 Based on the analysis of the deformation characteristics of Shuping landslide and the GA-LSSVM model above and due to
4 the obvious nonlinear and **episodic movement** deformation characteristics of monitoring stations ZG85, ZG86 and ZG87, we select
5 only these stations along longitudinal section A-B to verify and establish the prediction model. The model includes information
6 regarding rainfall, the reservoir water level, human activities and the long-term behavior of Shuping landslide. Because the
7 integrity of the data collected at monitoring points has an effect on the displacement prediction, the monitoring data from July
8 2003 to October 2013 are selected to explore landslide deformation. The data before October 2012 are used to train the
9 GA-LSSVM model, and the data after October 2012 are used to test the model.

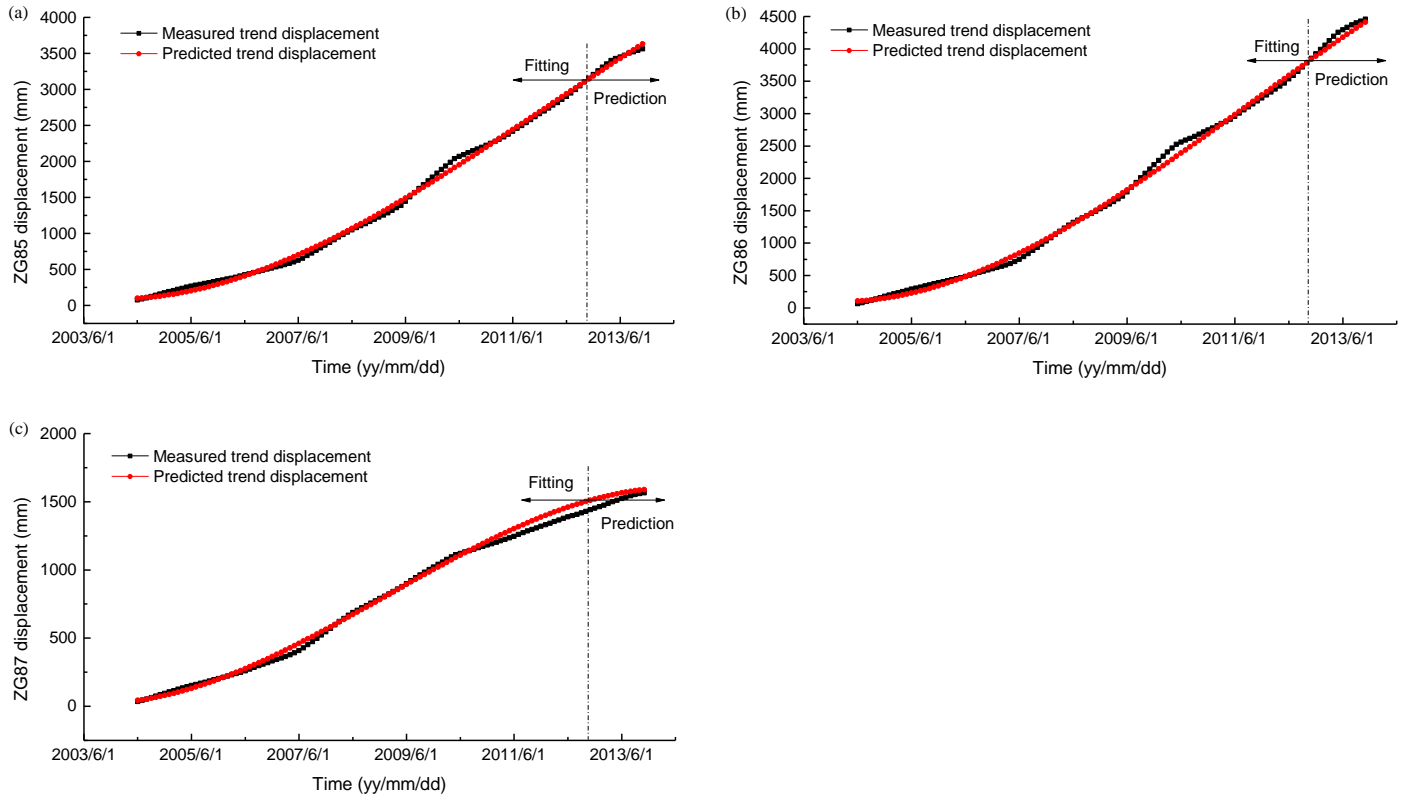
10 **4.1 Prediction of the trend component displacement**

11 Due to the scheduling period of the reservoir and the rainfall cycle, we choose 12 months as the moving average period.
12 Because the curves of the trend component displacement versus time have quasi-linear and incremental characteristics, we use
13 polynomial functions to fit these curves and provide the best-fitted results. The predicted and measured results of the trend
14 component displacement at monitoring stations ZG85, ZG86 and ZG87 are shown in Figs. 9(a), 9(b) and 9(c), respectively. They
15 indicate that the polynomial function provides good prediction performance for the trend component displacement and the fitted
16 functions are expressed in Eqs. (13), (14) and (15).

17
$$p_t = -0.0015t^3 + 0.4744t^2 - 8.4975t + 128.83 \quad R^2=0.9980 \quad (13)$$

18
$$p_t = -0.002t^3 + 0.604t^2 - 10.468t + 143.35 \quad R^2=0.9978 \quad (14)$$

19
$$p_t = -0.0015t^3 + 0.3088t^2 - 2.7227t + 29.832 \quad R^2=0.9976 \quad (15)$$



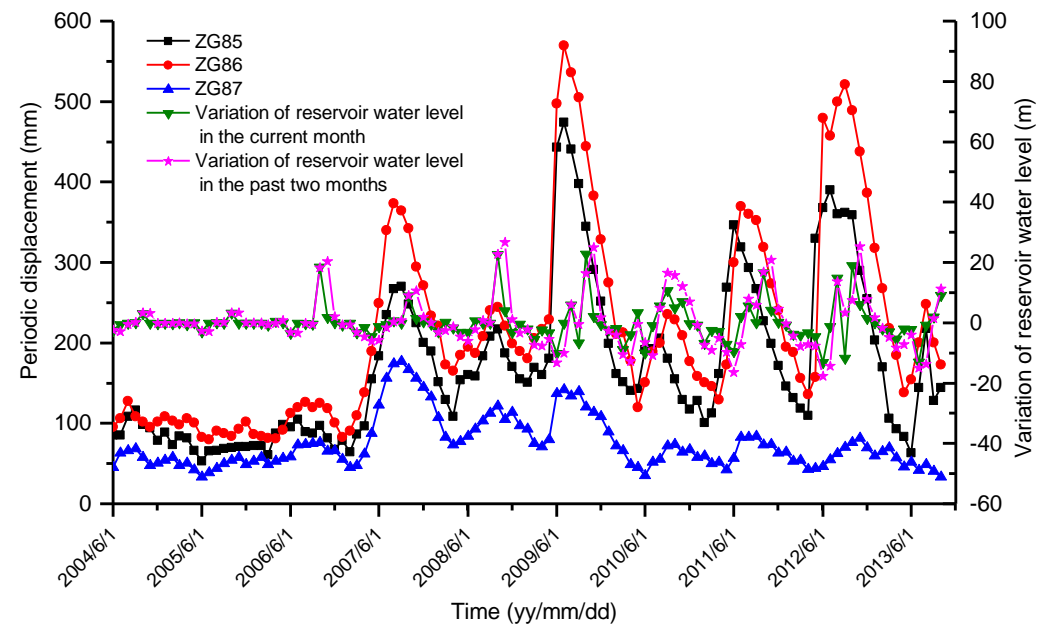
21 Fig. 9 Measured and predicted trend component displacement of Shuping landslide

22 **4.2 The predicted periodic component displacement**

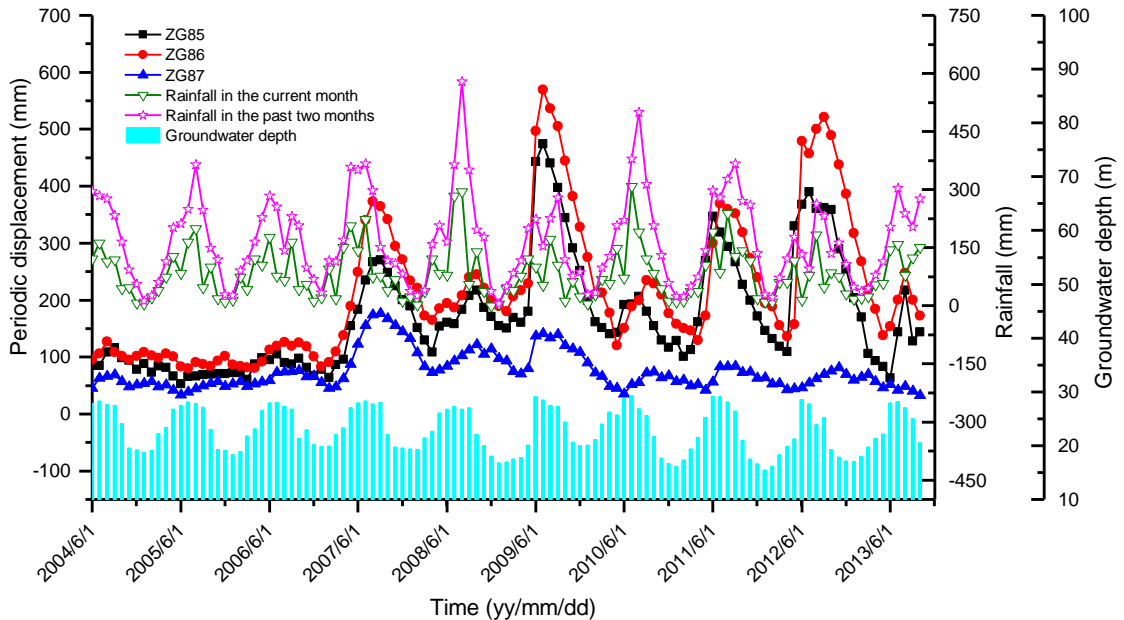
23 The periodic component displacement is determined by subtracting the extracted trend component displacement from the
24 cumulative displacement. The periodic displacement and the major influencing factors are illustrated in Figs. 10 and 11. The

1 variations in the periodic displacement are consistent with those in the influencing factors. The reservoir water level, rainfall and
 2 groundwater **significantly** influence the periodic displacement. For example, large periodic displacement can be observed in July
 3 2009 and September 2012 when the landslide was affected by heavy rainfall and large variations in reservoir water level. Although
 4 the variation in reservoir water level was small before April 2007, the periodic displacement still exhibited small fluctuations due
 5 to the effects of rainfall and groundwater. **This behavior could be explained in terms of stress changes within the landslide in that**
 6 **the rainfall events cause increased pore water pressures in the landslide shear zone which reduced the effective stress and increased**
 7 **instability.** After April 2007, several **distinct** peaks can be observed in the periodic displacement-time curves during periods of
 8 decreasing reservoir water level. For example, the periodic displacement increased from May to July 2009 and from May to
 9 September 2012. However, when the reservoir water level increased from 145 m to 175 m, the periodic displacement gradually
 10 decreased. **The main reason for the above conditions was that the rise of the reservoir water level increased the confining stress on**
 11 **the surface of the landslide and the hydrodynamic pressure, the direction of which was toward the interior of sliding body.**
 12 **Similarly, the lowering of the reservoir water level reduced the confining stress whilst pore water pressures were still high which**
 13 **would promote accelerated movement.** The periodicity of the rainfall also affected the **displacement rate.** The periodic
 14 displacement increased with increasing rainfall and reached a peak value in summer, which reflects a certain lag.

15 At the head scarp of the landslide at an elevation of 181m, groundwater depth was measured by water level sensor within
 16 inclinometer monitoring hole QZK3. The change in groundwater depth exhibits considerable agreement with rainfall and reservoir
 17 water level fluctuations, with a slight lag observed for the latter. Due to the slight lag with the reservoir water level, groundwater
 18 increased the hydrodynamic pressure during periods when the reservoir water level decreased or remained stable, which resulted in
 19 continuous deformation of the landslide. Therefore, in the shallow groundwater zone, the periodic displacements measured at the
 20 three monitoring stations exhibited considerable fluctuations. In conclusion, the results in Figs. 10 and 11 **indicate** that the
 21 reservoir water level **exerts the most influences on the displacement rate.**



22
 23 Fig. 10 The relationship between reservoir water level and the periodic displacement at GPS monitoring stations



1 Fig. 11 The relationships between rainfall, groundwater depth and periodic displacement at GPS monitoring stations

2 The grey relational grade can represent the proximity degree between two series. If the trends in the two series are consistent
3 or the degree of synchronous change is high, then the relational grade associated with system development is large. Otherwise, the
4 relational grade is small. To remove the influence of dimensional data, data series must be normalized before calculating the
5 relational grades, including the series of periodic displacement, rainfall and reservoir water level changes. The normalized formula
6 can be expressed by Eq. (16):

$$8 \quad \bar{y} = \frac{y - y_{\min}}{y_{\max} - y_{\min}} \quad (16)$$

9 where \bar{y} is the normalized value, y is the original value, y_{\max} is the maximum value of the data series, and y_{\min} is the
10 minimum value of the data series.

11 The grey relational coefficient of each data series and reference data series at each moment can be calculated as the
12 following:

$$13 \quad \gamma(y_0(k), y_i(k)) = \frac{\Delta \min + \rho \Delta \max}{\Delta_{o_j}(k) + \rho \Delta \max} \quad (17)$$

14 where $j=1,2\dots n$; $k=1,2\dots m$, n is the number of data series items and m is the number of parameters, $y_0(k)$ is the reference data
15 series, $y_j(k)$ is the series after data preprocessing, $\Delta_{o_j}(k) = \|y_0(k) - y_j(k)\|$ is the absolute value of the difference between $y_0(k)$
16 and $y_j(k)$, $\Delta \min = \min_{\forall j \in i} \min_{\forall k} \|y_0(k) - y_j(k)\|$ is the smallest value of $y_j(k)$, $\Delta \max = \max_{\forall j \in i} \max_{\forall k} \|y_0(k) - y_j(k)\|$ is the
17 largest value of $y_j(k)$, ρ is the distinguishing coefficient, $\rho \in [0,1]$. The smaller a value of ρ is, the larger the distinguished
18 ability is. $\rho = 0.5$ is generally used in the paper.

19 Then the average value of the grey relational coefficients is regarded as the grey relational grade (Tosun 2006). Thus, the
20 grey relational grade is generated as follows:

$$21 \quad \bar{\gamma}_j = \frac{1}{k} \sum_{i=1}^m \gamma_{ij} \quad (18)$$

1 where $\bar{\gamma}_j$ is the grey relational grade for the j th data series.

2 Based on the grey relational analysis method, the relational grades between the influencing factors and the periodic
 3 displacements are shown in Table 1. We can use the large grey relational grades as the input variables in the GA-LSSVM model.
 4 When the relational grade is larger than 0.6, the influencing factor is closely correlated with the periodic displacement, which
 5 suggests that the selection of the influencing factor for predicting periodic displacement is reasonable (Wang 2003; Wang et al.
 6 2004). Therefore, considering the characteristics of the periodic displacement and the relational grades between variables, the
 7 cumulative rainfall in the current month, the cumulative rainfall in the past two months, the reservoir water level, the variation in
 8 the reservoir water level in the current month, the variation in the reservoir water level in the past two months, and groundwater
 9 depth are selected as input variables. Moreover, the periodic component displacement is established as the output variable for use
 10 in the GA-LSSVM model.

11 Table 1 Relational grades between input variables and the periodic displacements

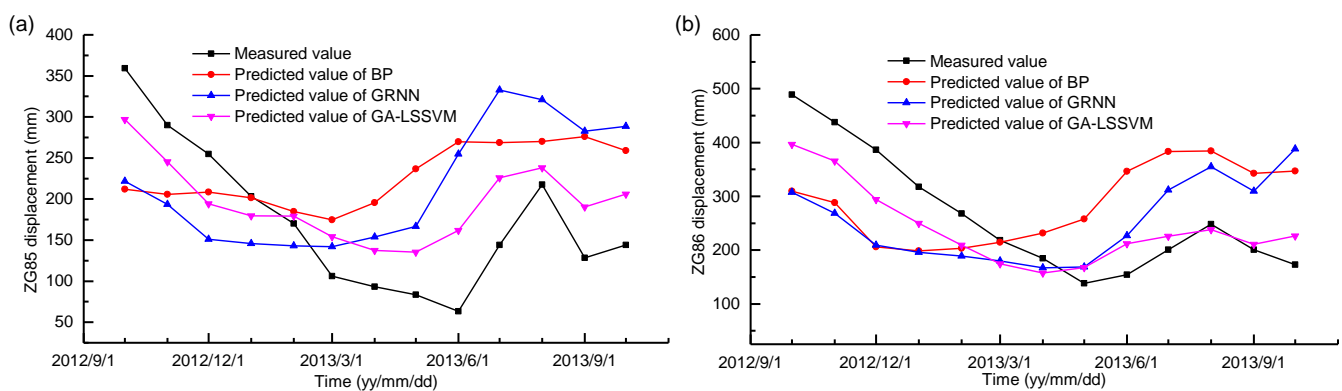
Monitoring station	Relational grade					
	The cumulative rainfall in the current month	The cumulative rainfall in the past two months	The reservoir water level	The variation of The reservoir water level in the current month	The variation of The reservoir water level in the past two months	Groundwater depth
ZG85	0.700	0.705	0.763	0.797	0.768	0.718
ZG86	0.682	0.691	0.756	0.794	0.770	0.714
ZG87	0.692	0.705	0.724	0.794	0.780	0.720

12 The parameters of the LSSVM are optimized by the GA, including the best values of C and σ . Table 2 shows the optimal
 13 parameters of the LSSVM. The maximum generation threshold of the GA is 200, and the population number is 20. To validate the
 14 prediction ability of the GA-LSSVM model, we compare the results of generalized regression neural network (GRNN) and back
 15 propagation (BP) with two hidden layers with the result of the GA-LSSVM model. In this paper, the smoothing factor of the
 16 GRNN is 0.48, and there are 10 nodes in one of the hidden layers and 11 nodes in the other hidden layer of the BP.

17 Table 2 Optimal parameters of the LSSVM model

Number	Monitoring station	C	σ
1	ZG85	11.8234	6.4122
2	ZG86	4.7346	8.0545
3	ZG87	39.7819	5.7981

18 The prediction results of the periodic component displacement are shown in Fig. 12. The predicted values of the three
 19 prediction models and the measured values are consistent and illustrate similar trends. However, the predicted values obtained
 20 using the GA-LSSVM exhibit better agreement with observations than the other methods. Notably, the advantages of the model are
 21 clear from April 2013 to October 2013, as the periodic component displacement exhibited good agreement with the major
 22 influencing factors during a period of heavy rainfall and large fluctuations in the reservoir water level.



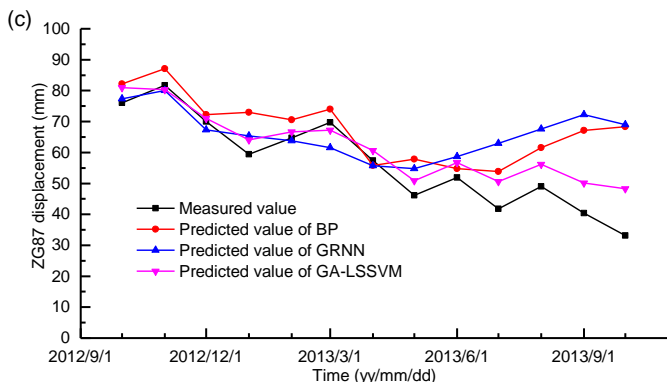


Fig. 12 Measured displacement and predicted periodic displacement of Shuping landslide

4.3 Predicted cumulative displacement

The predicted cumulative displacement is determined from the sum of the predicted trend displacement and the predicted periodic displacement. The predicted cumulative displacements and the measured values are presented in Table 3, Table 4 and Table 5 for monitoring station ZG85, ZG86 and ZG87, respectively. The results given in Table 3, Table 4 and Table 5 suggest that the GA-LSSVM model has better prediction performance than the GRNN model and the BP model, with a smaller relative error. Comparisons between the predicted values of cumulative displacement and measured values are shown in Fig. 13. The diagonal line shows the best prediction result in Fig. 13. The results are underestimated if the predicted values are located below the diagonal line, whereas the predicted values located above the line are overestimated. The predicted values from all the monitoring stations show good consistency with the measured values, as shown in Fig. 13.

Table 3 Comparison between the predicted values of cumulative displacement and measured values at monitoring station ZG85

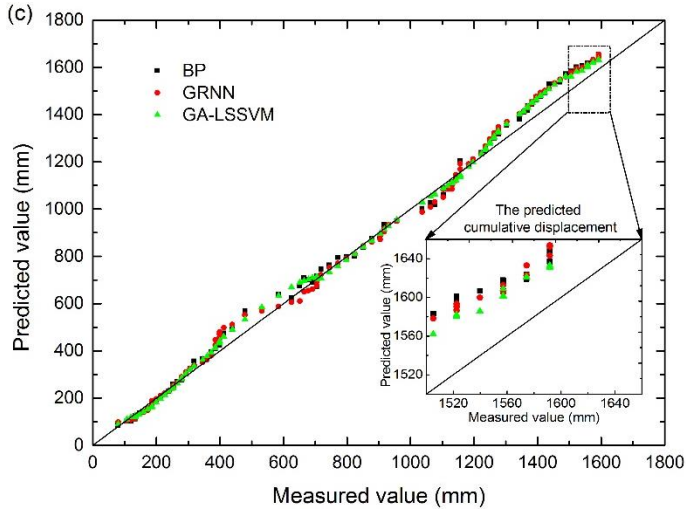
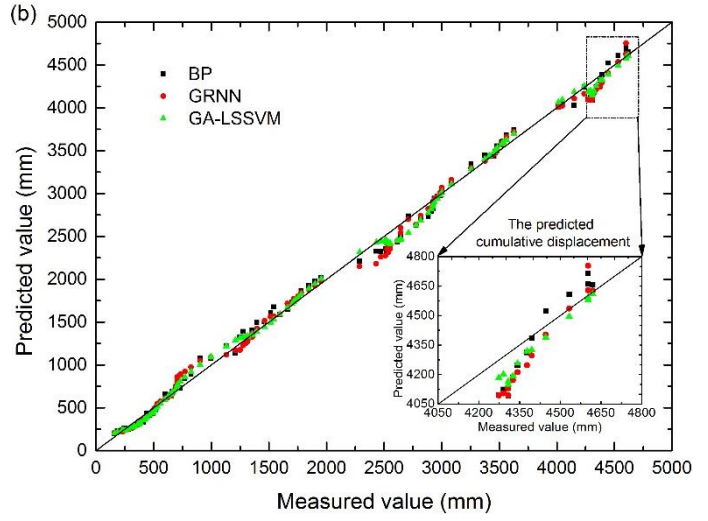
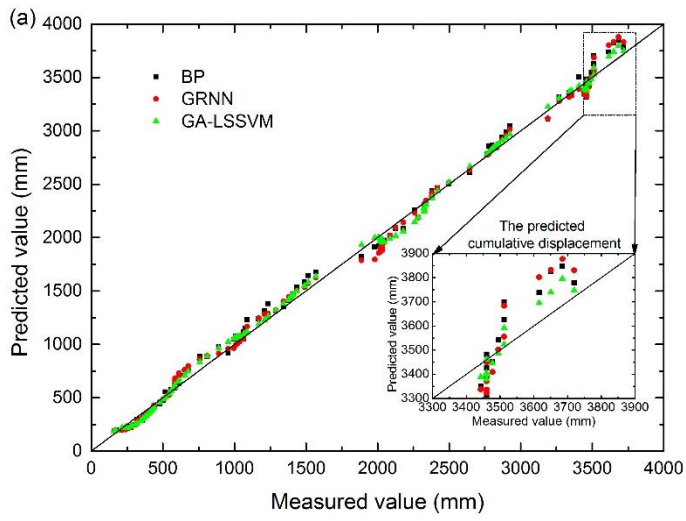
Time	Measured value (mm)	GA-LSSVM		GRNN		BP	
		Predicted value (mm)	Relative error (%)	Predicted value (mm)	Relative error (%)	Predicted value (mm)	Relative error (%)
2012/10/1	3460.208	3399.937	1.74	3324.829	3.91	3315.157	4.38
2012/11/1	3442.907	3389.608	1.55	3337.861	3.05	3349.827	2.78
2012/12/1	3460.208	3379.418	2.33	3336.503	3.58	3393.732	1.96
2013/1/1	3460.208	3406.014	1.57	3371.989	2.55	3427.727	0.95
2013/2/1	3477.509	3446.374	0.90	3410.133	1.94	3452.011	0.74
2013/3/1	3460.208	3462.169	0.06	3449.721	0.30	3482.668	0.64
2013/4/1	3494.81	3485.798	0.26	3502.356	0.22	3543.963	1.39
2013/5/1	3512.111	3524.423	0.35	3555.754	1.24	3625.738	3.13
2013/6/1	3512.111	3591.262	2.25	3684.274	4.90	3699.022	5.05
2013/7/1	3615.917	3695.444	2.20	3802.473	5.16	3738.225	3.27
2013/8/1	3719.723	3747.513	0.75	3830.496	2.98	3779.618	1.58
2013/9/1	3650.519	3740.002	2.45	3832.151	4.98	3825.664	4.58
2013/10/1	3685.121	3795.259	2.99	3877.587	5.22	3848.299	4.24

Table 4 Comparison between the predicted values of cumulative displacement and measured values at monitoring station ZG86

Time	Measured value (mm)	GA-LSSVM		GRNN		BP	
		Predicted value (mm)	Relative error (%)	Predicted value (mm)	Relative error (%)	Predicted value (mm)	Relative error (%)
2012/10/1	4273.356	4183.984	2.09	4094.396	4.19	4096.849	4.13
2012/11/1	4290.657	4201.857	2.07	4104.93	4.33	4124.839	3.86
2012/12/1	4307.958	4149.796	3.67	4094.607	4.95	4091.602	5.02
2013/1/1	4307.958	4164.444	3.33	4130.77	4.11	4133.425	4.05
2013/2/1	4325.26	4192.775	3.06	4172.182	3.54	4186.816	3.20
2013/3/1	4342.561	4256.46	1.98	4212.082	3.00	4246.771	2.21
2013/4/1	4377.163	4317.892	1.35	4247.617	2.96	4312.109	1.49
2013/5/1	4394.464	4326.232	1.55	4297.626	2.20	4386.529	0.18
2013/6/1	4446.367	4388.693	1.30	4403.464	0.96	4523.094	1.73
2013/7/1	4532.872	4495.404	0.83	4535.948	0.07	4607.573	1.65
2013/8/1	4619.377	4609.902	0.21	4626.647	0.16	4656.543	0.80
2013/9/1	4602.076	4579.721	0.49	4628.676	0.58	4661.733	1.30
2013/10/1	4602.076	4592.204	0.21	4754.15	3.30	4713.128	2.41

1 Table 5 Comparison between the predicted values of cumulative displacement and measured values at monitoring station ZG87

Time	Measured value (mm)	GA-LSSVM		GRNN		BP	
		Predicted value (mm)	Relative error (%)	Predicted value (mm)	Relative error (%)	Predicted value (mm)	Relative error (%)
2012/10/1	1505.19	1561.869	3.77	1578.221	4.85	1583.026	5.17
2012/11/1	1522.491	1580.602	3.82	1590.364	4.46	1597.352	4.92
2012/12/1	1522.491	1580.359	3.80	1586.605	4.21	1591.506	4.53
2013/1/1	1522.491	1581.923	3.90	1593.249	4.65	1600.855	5.15
2013/2/1	1539.792	1585.652	2.98	1599.822	3.90	1606.609	4.34
2013/3/1	1557.093	1600.959	2.82	1605.274	3.09	1617.769	3.90
2013/4/1	1557.093	1601.648	2.86	1606.713	3.19	1606.812	3.19
2013/5/1	1557.093	1608.744	3.32	1612.571	3.56	1615.702	3.76
2013/6/1	1574.394	1620.881	2.95	1622.897	3.08	1618.934	2.83
2013/7/1	1574.394	1620.703	2.94	1632.984	3.72	1623.904	3.14
2013/8/1	1591.696	1631.651	2.51	1643.08	3.23	1637.051	2.85
2013/9/1	1591.696	1630.511	2.44	1652.604	3.83	1647.566	3.51
2013/10/1	1591.696	1633.119	2.60	1653.808	3.90	1653.139	3.86



2

3

4 Fig. 13 Measured values versus predicted values of the cumulative displacement: (a) monitoring station ZG85, (b) monitoring station ZG86, and (c) monitoring station ZG87

5 Verification and error analyses

6 Three loss functions are used to assess the prediction performance and accuracy of the proposed model: the root mean square error (*RMSE*), mean absolute error (*MAE*), and mean absolute percentage error (*MAPE*). Then, the optimal parameters with minimum error are used to train the LSSVM model. The *RMSE*, *MAE* and *MAPE* formulas are as follows:

$$1 \quad RMSE = \sqrt{\frac{1}{n} \sum_{i=1}^n (s_i - s_i^*)^2} \quad (19)$$

$$2 \quad MAE = \frac{1}{n} \sum_{i=1}^n |s_i - s_i^*| \quad (20)$$

$$3 \quad MAPE = \frac{1}{n} \sum_{i=1}^n \left| \frac{s_i - s_i^*}{s_i} \right| \quad (21)$$

4 where s_i is the measured value, s_i^* is the predicted value, and n is the number of predicted values.

5 The performances of different models for landslide displacement prediction are assessed based on the *RMSE*, *MAE* and
 6 *MAPE*, as presented in Table 6. The prediction precision of the GA-LSSVM model based on time series analysis is better than that
 7 of the GRNN and the BP. Notably, the *RMSE*, *MAE* and *MAPE* values of the GA-LSSVM model were 63.4076, 56.6098 and
 8 1.587% lower than those of the GRNN model, respectively, and 49.3696, 43.5537 and 1.225% lower than those of the BP model
 9 for monitoring station ZG85. The predicted results for monitoring stations ZG86 and ZG87 exhibited similar trends. According to
 10 the prediction results, the GA-LSSVM model has good deduction ability for landslide displacement prediction and can provide
 11 assistance in early risk assessment and landslide forecasting.

12 Table 6 Comparison of the performance of cumulative displacement prediction for the three models

Model	RMSE (mm)			MAE (mm)			MAPE (%)		
	ZG85	ZG86	ZG87	ZG85	ZG86	ZG87	ZG85	ZG86	ZG87
GA-LSSVM	62.4146	87.7215	49.0485	53.0048	74.0601	48.5392	1.492	1.703	3.131
GRNN	125.8222	134.6764	59.8173	109.6146	115.1067	59.2756	3.079	2.643	3.821
BP	111.7842	123.1948	62.0223	96.5585	107.6724	60.9701	2.717	2.464	3.935

13 6 Conclusion

14 Landslide displacement prediction is a major focus of contemporary landslide research. We use the deformation of a
 15 episodic movement landslide (Shuping landslide) as an example. According to time series analysis, the cumulative displacement is
 16 decomposed into a trend component displacement representing the trend of landslide deformation in the long term and a periodic
 17 component displacement that represents short-term deformation fluctuations. The trend displacement and periodic displacement
 18 are predicted using a polynomial function and the GA-LSSVM model, respectively. The LSSVM yields good fitting results in
 19 predicting the periodic displacement with the GA, which is utilized to determine the optimal parameters of the LSSVM. Based on
 20 our analysis of the deformation of Shuping landslide, the reservoir water level, rainfall and groundwater have major influences on
 21 the cumulative displacement. Therefore, based on the relational grades, we select six influential factors as the input variables. The
 22 predicted cumulative displacement is obtained from the sum of the predicted trend displacement and the predicted periodic
 23 displacement.

24 The GA-LSSVM model displays the highest accuracy, the smallest *RMSE* of 62.4146 mm, the smallest *MAE* of 53.0048 mm,
 25 and the smallest *MAPE* of 1.492% at monitoring station ZG85, while these three values are 87.7215 mm, 74.0601 mm and 1.703%
 26 at monitoring station ZG86 and 49.0485 mm, 48.5392 mm and 3.131% at monitoring station ZG87. The study results show that
 27 GA-LSSVM provides good performance for landslide displacement prediction, and the GA is appropriate for determining the
 28 optimal parameters used in the LSSVM model. Thus, the GA-LSSVM model can be effectively used to predict landslide
 29 displacement and reflect the corresponding relationships between the major influencing factors and the periodic component
 30 displacement.

31 Acknowledgments

32 The authors would like to acknowledge gratefully the Editor and the anonymous reviewers for their constructive criticism on
 33 the earlier version of this paper and offering valuable suggestions that contributed to its improvement. This study was supported by
 34 National Natural Science Foundation of China, Key Project of National Science Foundation of China (No. 41230637, No.
 35 41502290), the Ministry of Science and Technology of the P. R. China, National Basic Research Program of China (973 Program)

1 (2011CB710600).

2

3 References

4 Abdi, M. J., and Giveki, D.: Automatic detection of erythematous-squamous diseases using PSO-SVM based on association rules,
5 Eng Appl Artif Intel, 26, 603-608, 10.1016/j.engappai.2012.01.017, 2013.

6 Ahmed, B.: Landslide susceptibility mapping using multi-criteria evaluation techniques in Chittagong Metropolitan Area,
7 Bangladesh, Landslides, 6, 1077-1095, 10.1007/s10346-014-0521-x, 2013.

8 Ali Ahmadi, M., Zendehboudi, S., Lohi, A., Elkamel, A., and Chatzis, I.: Reservoir permeability prediction by neural networks
9 combined with hybrid genetic algorithm and particle swarm optimization, Geophys Prospect, 61, 582-598,
10 10.1111/j.1365-2478.2012.01080.x, 2013.

11 Altinel, B., Can Ganiz, M., and Diri, B.: A corpus-based semantic kernel for text classification by using meaning values of terms,
12 Eng Appl Artif Intel, 43, 54-66, 10.1016/j.engappai.2015.03.015, 2015.

13 Brockwell, P. J., and Davis, R. A.: Time series: theory and methods, Springer Science & Business Media, 2013.

14 Cao, Y., Yin, K., Alexander, D. E., and Zhou, C.: Using an extreme learning machine to predict the displacement of step-like
15 landslides in relation to controlling factors, Landslides, 4, 725-736, 10.1007/s10346-015-0596-z, 2016.

16 Corominas, J., Moya, J. E., Ledesma, A., Lloret, A., and Gili, J. A.: Prediction of ground displacements and velocities from
17 groundwater level changes at the Vallcebre landslide (Eastern Pyrenees, Spain, Landslides, 2, 83-96, 10.1007/s10346-005-0049-1,
18 2005.

19 Desai, C. S., Samtani, N. C., Vulliet, L.: Constitutive modeling and analysis of creeping slopes, J Geotech Eng Trans ASCE,
20 121, 43-56, 10.1061/(ASCE)0733-9410(1995)121:1(43), 1995.

21 Du, J., Yin, K., and Lacasse, S.: Displacement prediction in colluvial landslides, Three Gorges Reservoir, China, Landslides, 10,
22 203-218, 10.1007/s10346-012-0326-8, 2013.

23 Duan, K., Keerthi, S. S., and Poo, A. N.: Evaluation of simple performance measures for tuning SVM hyperparameters,
24 Neurocomputing, 51, 41-59, 10.1016/S0925-2312(02)00601-X, 2013.

25 Elbisy, M. S.: Sea wave parameters prediction by support vector machine using a genetic algorithm, J Coastal Res, 314, 892-899,
26 10.2112/JCOASTRES-D-13-00087.1, 2015.

27 Farzan, A., Mashohor, S., Ramlı, A. R., and Mahmud, R.: Boosting diagnosis accuracy of Alzheimer's disease using high
28 dimensional recognition of longitudinal brain atrophy patterns, Behav Brain Res, 290, 124-130, 10.1016/j.bbr.2015.04.010, 2015.

29 Fei, S., Wang, M., Miao, Y., Tu, J., and Liu, C.: Particle swarm optimization-based support vector machine for forecasting
30 dissolved gases content in power transformer oil, Energ Convers Manage, 50, 1604-1609, 10.1016/j.enconman.2009.02.004, 2009.

31 Feng, X., Zhao, H., and Li, S.: Modeling non-linear displacement time series of geo-materials using evolutionary support vector
32 machines, Int J Rock Mech Min, 41, 1087-1107, 10.1016/j.ijrmms.2004.04.003, 2004.

33 Garg, A., and Tai, K.: A hybrid genetic programming-artificial neural network approach for modeling of vibratory finishing process,
34 International Proceedings of Computer Science and Information Technology (IPCSIT), 14-19, 2011.

35 Garg, A., and Tai, K.: Stepwise approach for the evolution of generalized genetic programming model in prediction of surface
36 finish of the turning process, Adv Eng Softw, 78, 16-27, 10.1016/j.advengsoft.2017.01.005, 2014.

37 Gelisli, K., Kaya, T., and Babacan, A. E.: Assessing the factor of safety using an artificial neural network: case studies on
38 landslides in Giresun, Turkey, Environ Earth Sci, 73, 8639-8646, 10.1007/s12665-015-4027-1, 2015.

39 Goetz, J. N., Brenning, A., Petschko, H., and Leopold, P.: Evaluating machine learning and statistical prediction techniques for
40 landslide susceptibility modeling, Comput Geosci-Uk, 81, 1-11, 10.1016/j.cageo.2015.04.007, 2015.

41 Gu, J., Zhu, M., and Jiang, L.: Housing price forecasting based on genetic algorithm and support vector machine, Expert Syst Appl,
42 38, 3383-3386, 10.1016/j.eswa.2010.08.123, 2011.

43 Guzzetti, F., Reichenbach, P., Cardinali, M., Galli, M., and Ardizzone, F.: Probabilistic landslide hazard assessment at the basin
44 scale, Geomorphology, 72, 272-299, 10.1016/j.geomorph.2005.06.002, 2005.

45 Hejazi, F., Toloue, I., Jaafar, M. S., and Noorzaei, J.: Optimization of earthquake energy dissipation system by genetic algorithm,
46 Comput-Aided Civ Infrastruct Eng, 28, 796-810, 10.1111/mice.12047, 2013.

1 Hong, H., Pradhan, B., Jebur, M. N., Bui, D. T., Xu, C., and Akgun, A.: Spatial prediction of landslide hazard at the Luxi area
2 (China) using support vector machines, *Environ Earth Sci*, 75, 10.1007/s12665-015-4866-9, 2016.

3 Hwang, S., Jeong, M. K., and Yum, B.: Robust relevance vector machine with variational inference for improving virtual
4 metrology accuracy, *Ieee T Semiconduct M*, 27, 83-94, 10.1109/TSM.2013.2286498, 2014.

5 Kavzoglu, T., Kutlug Sahin, E., and Colkesen, I.: An assessment of multivariate and bivariate approaches in landslide susceptibility
6 mapping: a case study of Duzkoy district, *Nat Hazards*, 76, 471-496, 10.1007/s11069-014-1506-8, 2015.

7 Kawabata, D., and Bandibas, J.: Landslide susceptibility mapping using geological data, a DEM from ASTER images and an
8 artificial neural network (ANN), *Geomorphology*, 113, 97-109, 10.1016/j.geomorph.2009.06.006, 2009.

9 Kirschbaum, D. B., Adler, R., Hong, Y., Hill, S., and Lerner-Lam, A.: A global landslide catalog for hazard applications: method,
10 results, and limitations, *Nat Hazards*, 3, 561-575, 10.1007/s11069-009-9401-4, 2010.

11 Koza, J. R.: *Genetic programming: on the programming of computers by means of natural selection*, MIT press, Cambridge, MA,
12 1992.

13 Lessmann, S., Stahlbock, R., and Crone, S. F.: Optimizing hyperparameters of support vector machines by genetic algorithms, Las
14 Vegas, CSREA Press, 2005.

15 Levasseur, S., Malécot, Y., Boulon, M., and Flavigny, E.: Soil parameter identification using a genetic algorithm, *Int J Numer Anal
16 Met*, 32, 189-213, 10.1002/nag.614, 2008.

17 Li, F., Tang, B. P., and Liu, W. Y.: Fault diagnosis based on least square support vector machine optimized by genetic algorithm,
18 *Journal of Chongqing University*, 33, 14-20, 2010(in Chinese).

19 Lian, C., Zeng, Z. G., Yao, W., and Tang, H. M.: Displacement prediction model of landslide based on a modified ensemble
20 empirical mode decomposition and extreme learning machine, *Nat Hazards*, 66, 759-771, 10.1007/s11069-012-0517-6, 2013.

21 Lian, C., Zeng, Z. G., Yao, W., and Tang, H. M.: Ensemble of extreme learning machine for landslide displacement prediction
22 based on time series analysis, *Neural Comput Appl*, 24, 99-107, 10.1007/s00521-013-1446-3, 2014.

23 Lian, C., Zeng, Z., Yao, W., and Tang, H.: Multiple neural networks switched prediction for landslide displacement, *Eng Geol*, 186,
24 91-99, 10.1016/j.enggeo.2014.11.014, 2015.

25 Lin, P. T.: *Support vector regression: Systematic design and performance analysis*, Department of Electronic Engineering, National
26 Taiwan University, 2001.

27 Liu, Z., Shao, J., Xu, W., Chen, H., and Shi, C.: Comparison on landslide nonlinear displacement analysis and prediction with
28 computational intelligence approaches, *Landslides*, 11, 889-896, 10.1007/s10346-013-0443-z, 2014.

29 Lv, Y., Liu, J., Yang, T., and Zeng, D.: A novel least squares support vector machine ensemble model for NO_x emission prediction
30 of a coal-fired boiler, *Energy*, 55, 319-329, 10.1016/j.energy.2013.02.062, 2013.

31 Marjanović, M., Kovačević, M., Bajat, B., and Voženílek, V.: Landslide susceptibility assessment using SVM machine learning
32 algorithm, *Eng Geol*, 123, 225-234, 10.1016/j.enggeo.2011.09.006, 2011.

33 Micheletti, N., Foresti, L., Kanevski, M., Pedrazzini, A., and Jaboyedoff, M.: Landslide susceptibility mapping using adaptive
34 support vector machines and feature selection, *Geophys Res Abstr, EGU*, 13, 2013.

35 Min, J. H., and Lee, Y.: Bankruptcy prediction using support vector machine with optimal choice of kernel function parameters,
36 *Expert Syst Appl*, 28, 603-614, 10.1016/j.eswa.2004.12.008, 2005.

37 Miyagi, T., Yamashina, S., Esaka, F., and Abe, S.: Massive landslide triggered by 2008 Iwate-Miyagi inland earthquake in the
38 Aratozawa Dam area, Tohoku, Japan, *Landslides*, 1, 99-108, 10.1007/s10346-010-0226-8, 2011.

39 Nefeslioglu, H. A., Gokceoglu, C., and Sonmez, H.: An assessment on the use of logistic regression and artificial neural networks
40 with different sampling strategies for the preparation of landslide susceptibility maps, *Eng Geol*, 97, 171-191,
41 10.1016/j.enggeo.2008.01.004, 2008.

42 Pourbasheer, E., Riahi, S., Ganjali, M. R., and Norouzi, P.: Application of genetic algorithm-support vector machine (GA-SVM)
43 for prediction of BK-channels activity, *Eur J Med Chem*, 44, 5023-5028, 10.1016/j.ejmchem.2009.09.006, 2009.

44 Pradhan, B., Abokharima, M. H., Jebur, M. N., and Tehrany, M. S.: Land subsidence susceptibility mapping at Kinta Valley
45 (Malaysia) using the evidential belief function model in GIS, *Nat Hazards*, 73, 1019-1042, 10.1007/s11069-014-1128-1, 2014.

46 Ren, F., Wu, X., Zhang, K., and Niu, R.: Application of wavelet analysis and a particle swarm-optimized support vector machine to

1 predict the displacement of the Shuping landslide in the Three Gorges, China, Environ Earth Sci, 73, 4791-4804,
2 10.1007/s12665-014-3764-x, 2015.

3 Sassa, K., Picarelli, L., and Yin, Y. P.: Monitoring, prediction and early warning. In: Sassa K, Canuti P (eds) Landslides-disaster
4 risk reduction, Springer-Verlag, Berlin Heidelberg, 2009.

5 Shen, J., Karakus, M., and Xu, C.: Direct expressions for linearization of shear strength envelopes given by the Generalized
6 Hoek-Brown criterion using genetic programming, Comput Geotech, 44, 139-146, 10.1016/j.comgeo.2012.04.008, 2012.

7 Sun, Z., Choi, T., Au, K., and Yu, Y.: Sales forecasting using extreme learning machine with applications in fashion retailing, Decis
8 Support Syst, 46, 411-419, 10.1016/j.dss.2008.07.009, 2008.

9 Suykens, J.A.K., and Vandewalle, J.: Least Squares Support Vector Machine Classifiers, Neural Process Lett 9, 293-300,
10 10.1023/A:1018628609742, 1999.

11 Suykens, J.A.K., De Brabanter, J., Lukas, L., and Vandewalle, J.: Weighted least squares support vector machines: robustness and
12 sparse approximation, Neurocomputing, 48, 85-105, 10.1016/S0925-2312(01)00644-0, 2002.

13 **Tosun N.: Determination of optimum parameters for multi-performance characteristics in drilling by using grey relational analysis,**
14 **The International Journal of Advanced Manufacturing Technology, 28, 450-455, 10.1007/s00170-004-2386-y, 2006.**

15 Turner, D., Lucieer, A., and de Jong, S.: Time series analysis of landslide dynamics using an unmanned aerial vehicle (UAV),
16 Remote Sens-Basel, 7, 1736-1757, 10.3390/rs70201736, 2015.

17 Vandenbergh, F., and Engelbrecht, A. P.: A study of particle swarm optimization particle trajectories, Inform Sciences, 176,
18 937-971, 10.1016/j.ins.2005.02.003, 2006.

19 Vapnik, V.: The nature of statistical learning theory, Springer Verlag, New York, 1995.

20 Wang, J. F.: Quantitative prediction of landslide using S-curve, Chin J Geol Hazard Control, 14, 3-10, 2003(in Chinese).

21 Wang, Y., Yin, K. L., and An, G. F.: Grey correlation analysis of sensitive factors of landslide, Rock Soil Mech, 25, 91-93, 2004(in
22 Chinese).

23 Xu, H., and Chen, G.: An intelligent fault identification method of rolling bearings based on LSSVM optimized by improved PSO,
24 Mech Syst Signal Pr, 35, 167-175, 10.1016/j.ymssp.2012.09.005, 2013.

25 Yao, W., Zeng, Z. G., Lian, C., and Tang, H. M.: Ensembles of echo state networks for time series prediction. In: Sixth
26 international conference on advanced computational intelligence, Hangzhou, China, 299-304, 2013.

27 Yin, X., and Yu, W.: The virtual manufacturing model of the worsted yarn based on artificial neural networks and grey theory, Appl
28 Math Comput, 185, 322-332, 10.1016/j.amc.2006.06.117, 2007.

29 Zhang, H., Luo, Y.Y., Zhang, L.T., and Chen, Z.: Cultivated land change forecast based on genetic algorithm and least squares
30 support vector machines, Transactions of the Chinese Society of Agricultural Engineering, 25, 226-231, 2009.

31 Zhang, W., Niu, P., Li, G., and Li, P.: Forecasting of turbine heat rate with online least squares support vector machine based on
32 gravitational search algorithm, Knowl-Based Syst, 39, 34-44, 10.1016/j.knosys.2012.10.004, 2013.

33

34